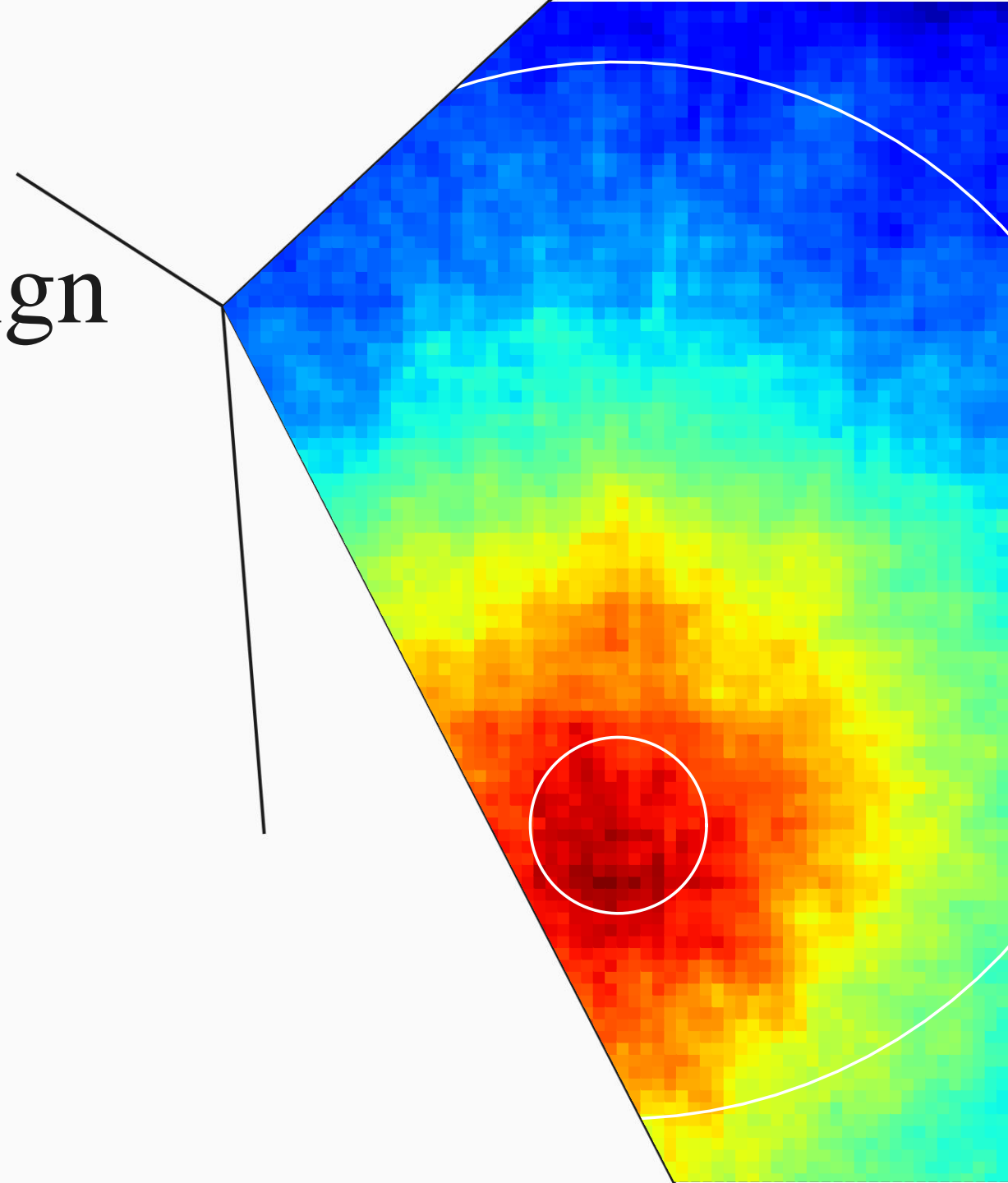


A Compton camera design for prompt gamma imaging during BNCT

K. Nutter, T. Price, Tz. Kokalova,
S. Green, B. Phoenix.

Corresponding email: kjn718@bham.ac.uk



Boron Neutron Capture Therapy (BNCT)

- Binary cancer therapy that utilises biological and physical targeting of the tumour
- Neutron capture produces short-range, high linear energy transfer (LET) particles
- Research has focused on brain, head and neck cancers

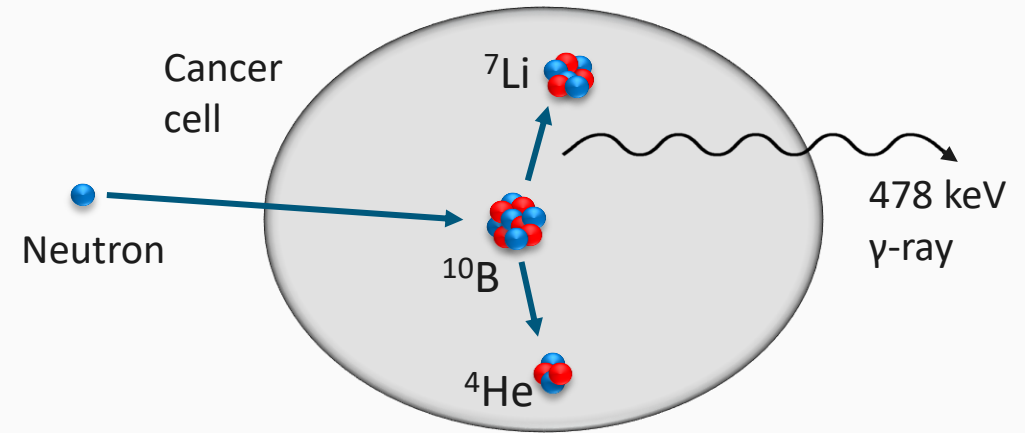


Fig 1. Visual representation of the fundamental interaction utilised during BNCT.

- Cross section for thermal neutron capture on ^{10}B is 3840 barns [1]

Boron Neutron Capture Therapy (BNCT)

- Binary cancer therapy that utilises

- **However, obtaining accurate dosimetry is challenging!!!**

- and neck cancers

neutron capture on ^{10}B is 3840 barns [1]

Prompt Gamma Imaging for BNCT

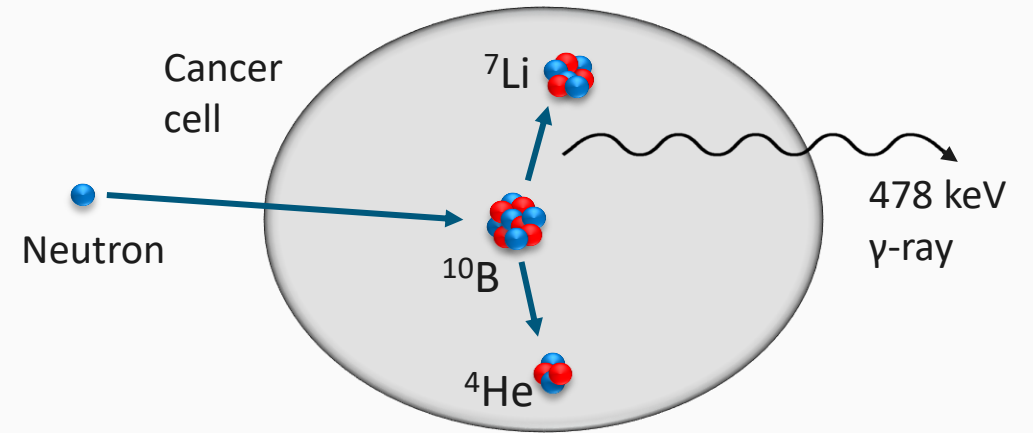


Fig 1. Visual representation of the fundamental interaction utilised during BNCT.

Prompt Gamma Imaging for BNCT

- A 478 keV prompt gamma ray is produced after 93.9% of the neutron capture interactions
- Delivered dose could be inferred by imaging the production vertices of these gamma rays

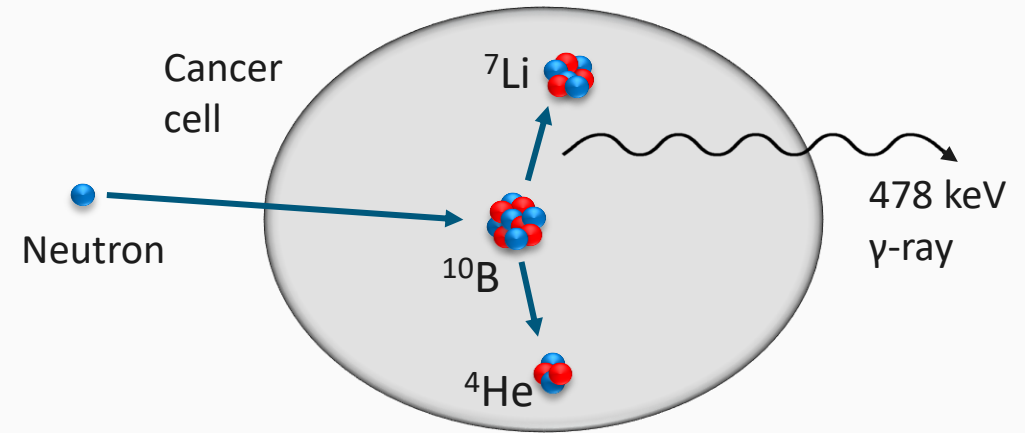
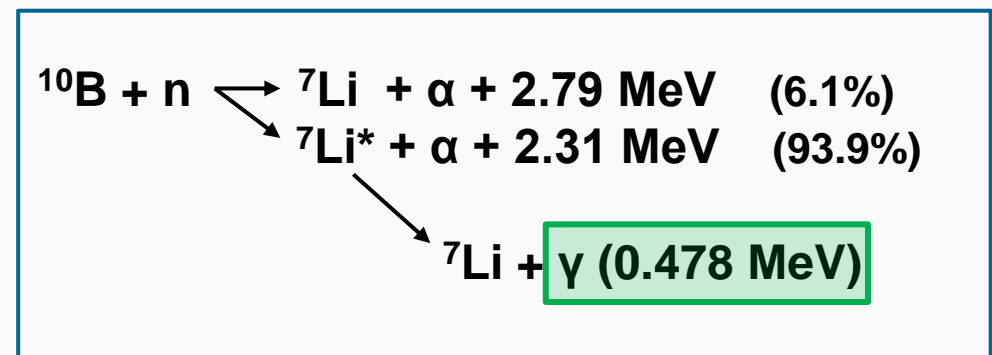


Fig 1. Visual representation of the fundamental interaction utilised during BNCT.



Prompt Gamma Imaging for BNCT

- A 478 keV prompt gamma ray is produced after 93.9% of the neutron capture interactions
- Delivered dose could be inferred by imaging the production vertices of these gamma rays
- Imaging could be done with SPECT or Compton camera systems

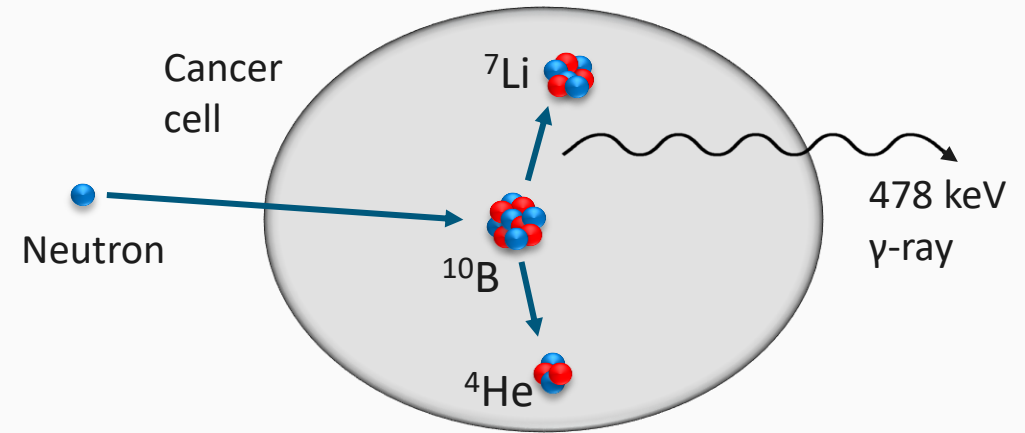
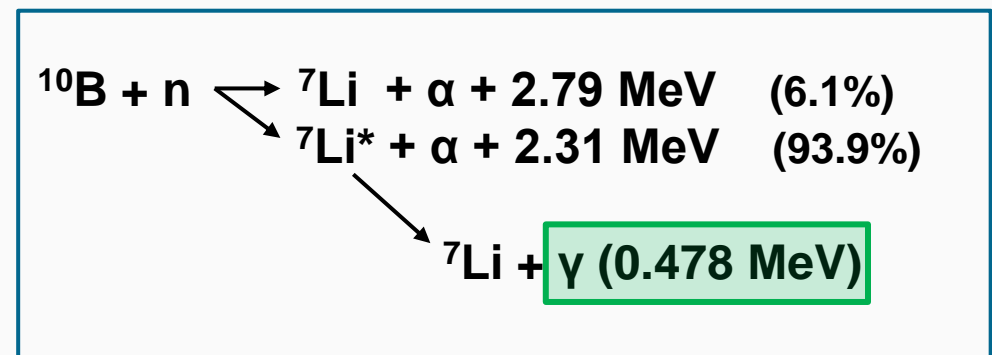
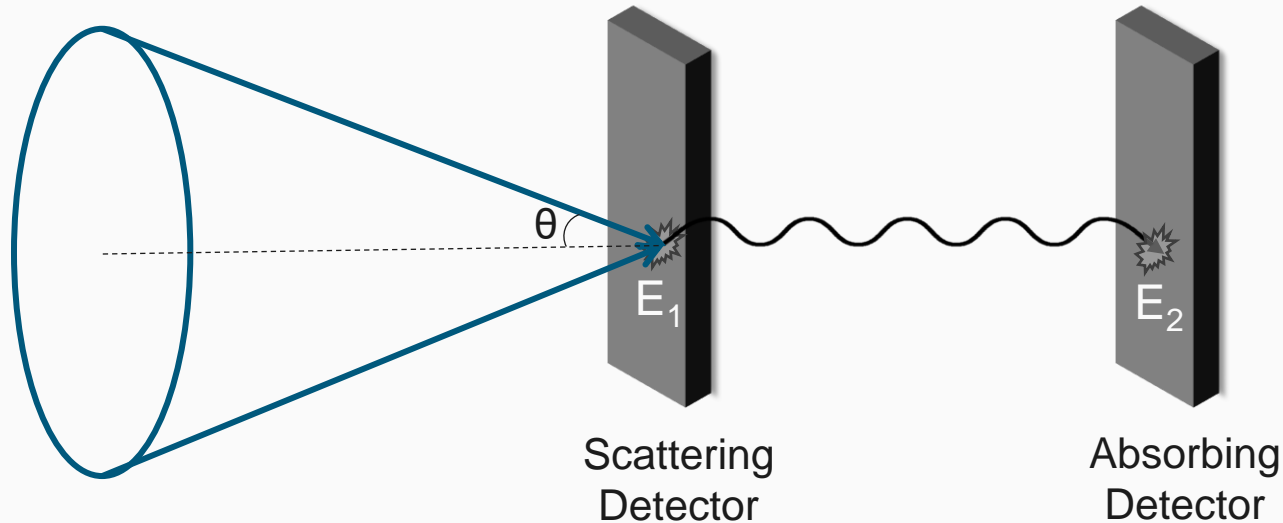


Fig 1. Visual representation of the fundamental interaction utilised during BNCT.



Compton Camera

- Combining axis between interaction points with scattering angle gives a **conical surface** from which the photon must have originated



$$\cos \theta = 1 - \frac{m_e c^2 E_1}{E_2 (E_1 + E_2)}$$

Fig 2. Principle of operation of a Compton camera.

Compton Camera

- Combining axis between interaction points with scattering angle gives a **conical surface** from which the photon must have originated

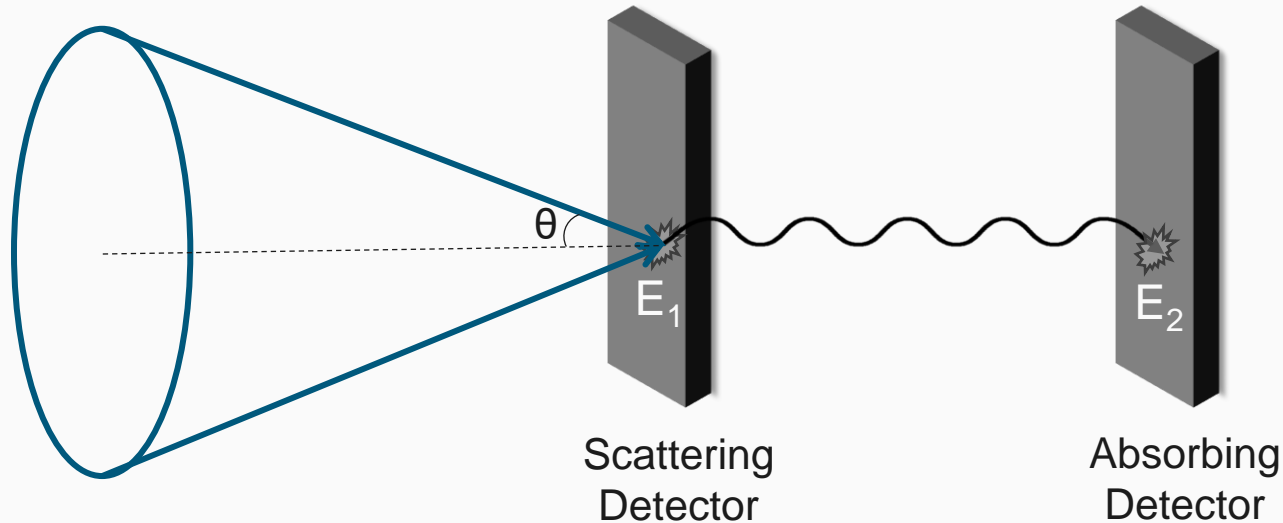


Fig 2. Principle of operation of a Compton camera.

$$\cos \theta = 1 - \frac{m_e c^2 E_1}{E_2 (E_1 + E_2)}$$

- ★ No reliance on mechanical collimation
- ★ Higher possible camera efficiencies

LaBr₃ Detector Array

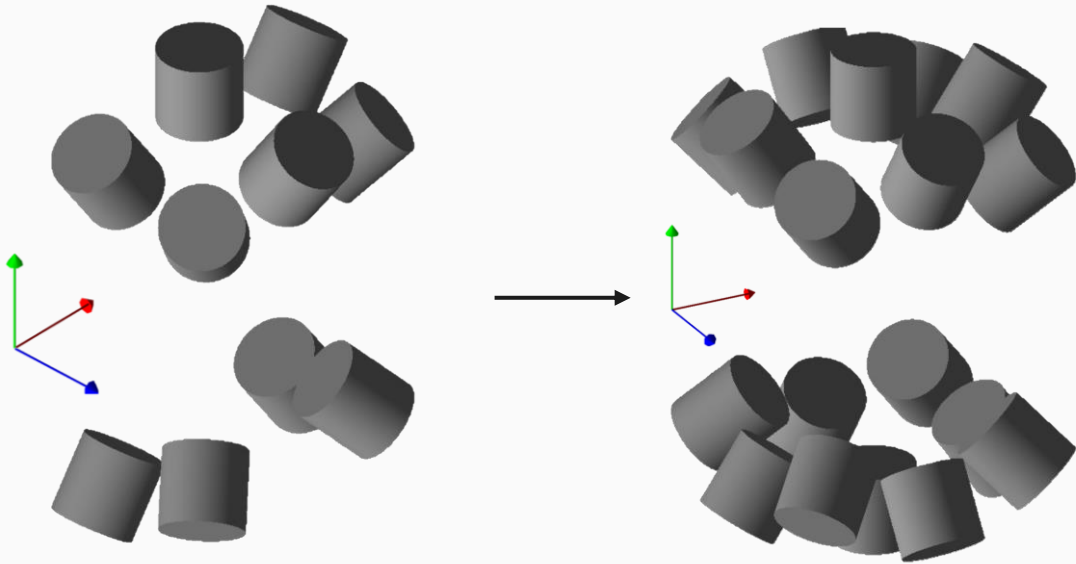


Fig 3. Original 10 detector array.

Fig 4. Extrapolated 18 detector array.

LaBr₃ Detector Array

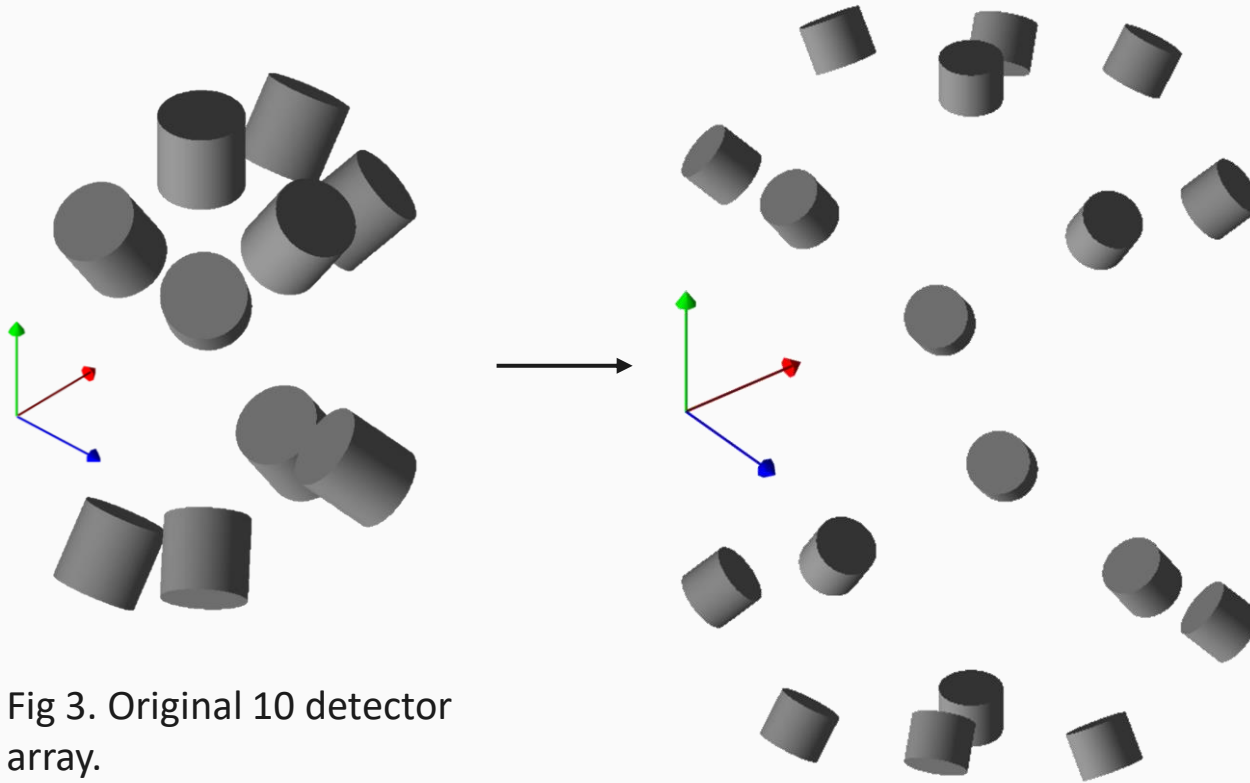
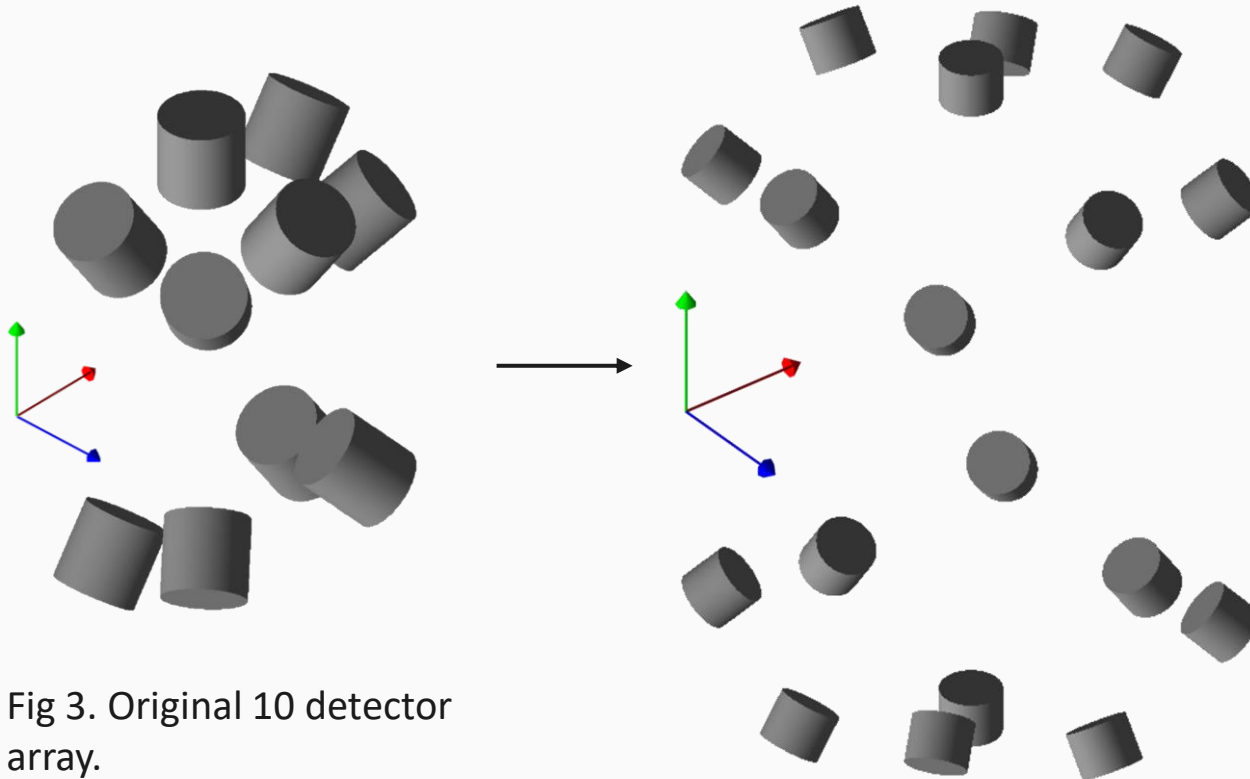


Fig 3. Original 10 detector array.

Fig 5. Extrapolated 18 detector array 30 cm from centre.

LaBr₃ Detector Array



- Each detector can act as a scattering and absorbing detector
- Requires large angle scatters

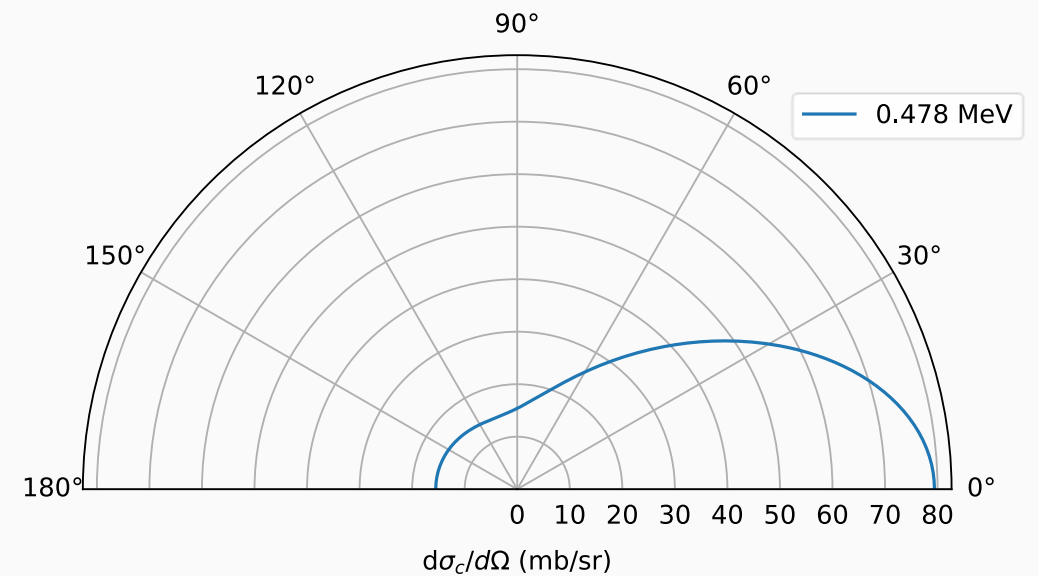


Fig 6. Klein-Nishina distribution for a 478 keV photon.

Modified Compton Camera Advantages

- Significantly increases the number of detection channels

Detection channel - a distinct pair of a scattering and absorbing detector.

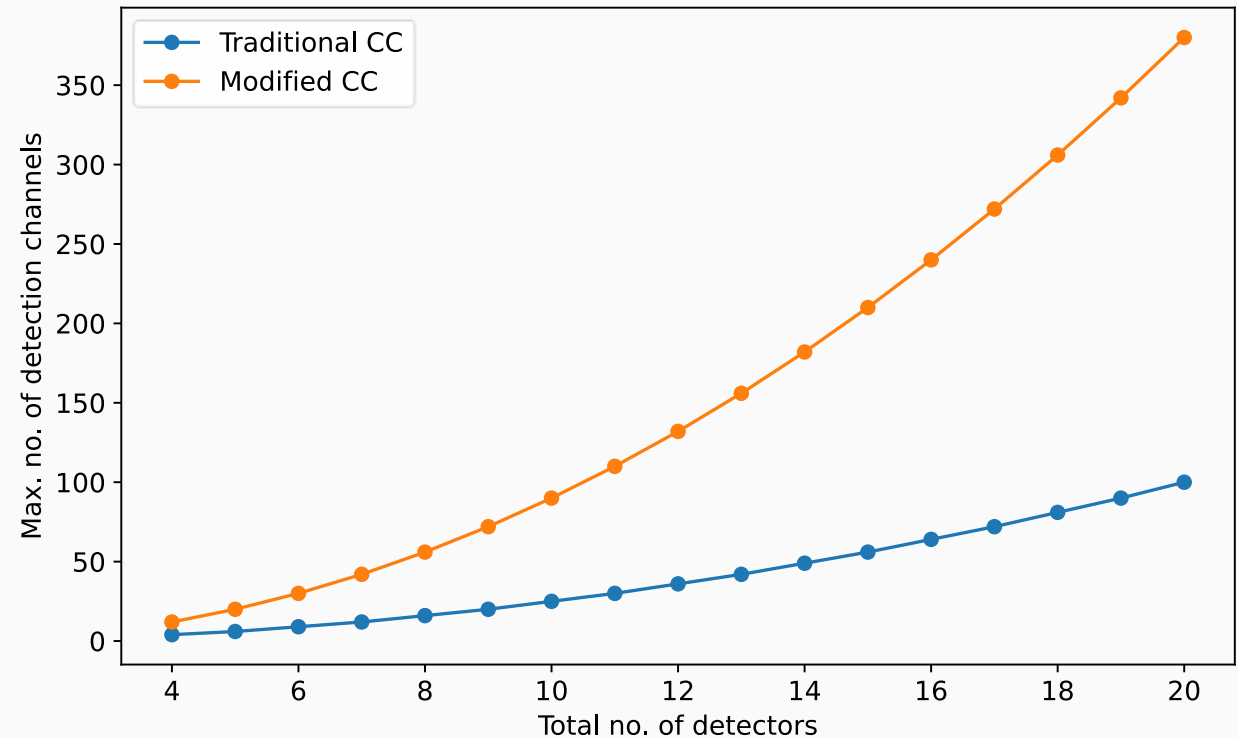


Fig 7. Maximum detection channels achieved when using a traditional and modified Compton camera design.

Modified Compton Camera Advantages

- Significantly increases the number of detection channels
- This increase helps to counteract lower scattering probability
- Greater variety of cones produced should improve spatial resolution

Detection channel - a distinct pair of a scattering and absorbing detector.

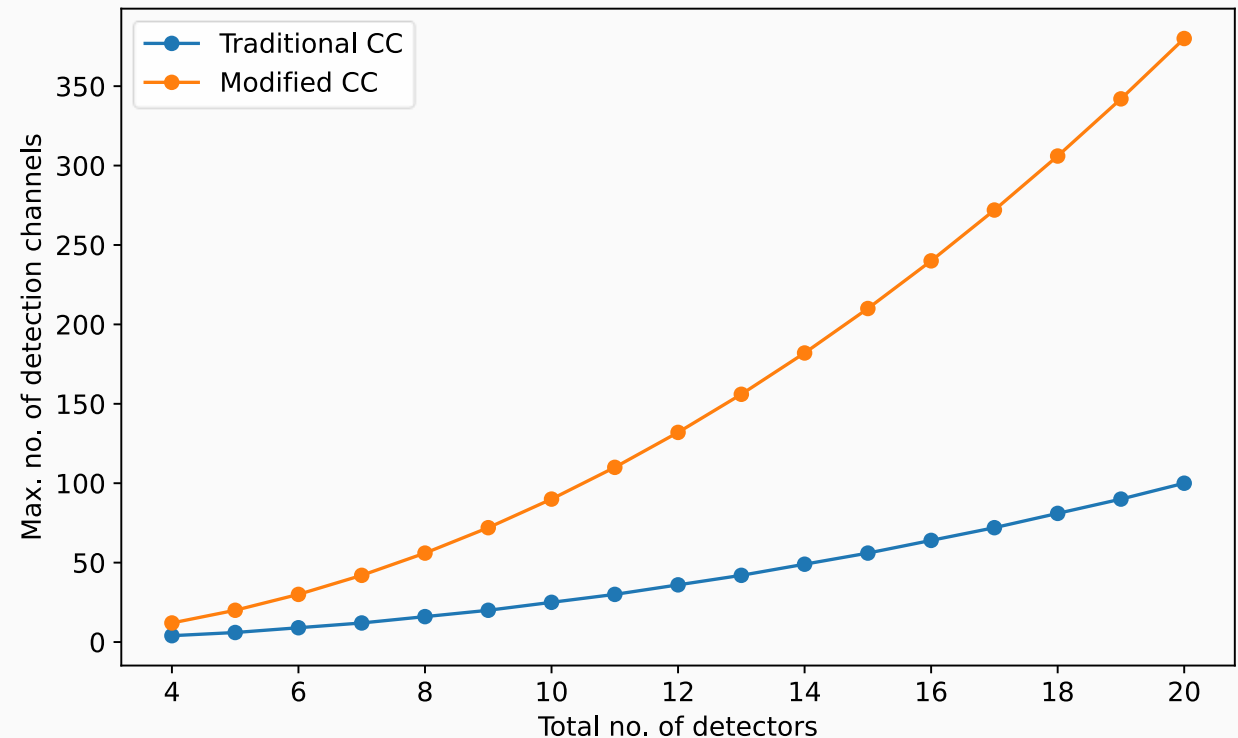


Fig 7. Maximum detection channels achieved when using a traditional and modified Compton camera design.

Simulation Setup

- Initial testing and validation of detector response using 478 keV point source
- Then introduced neutron beam and phantom

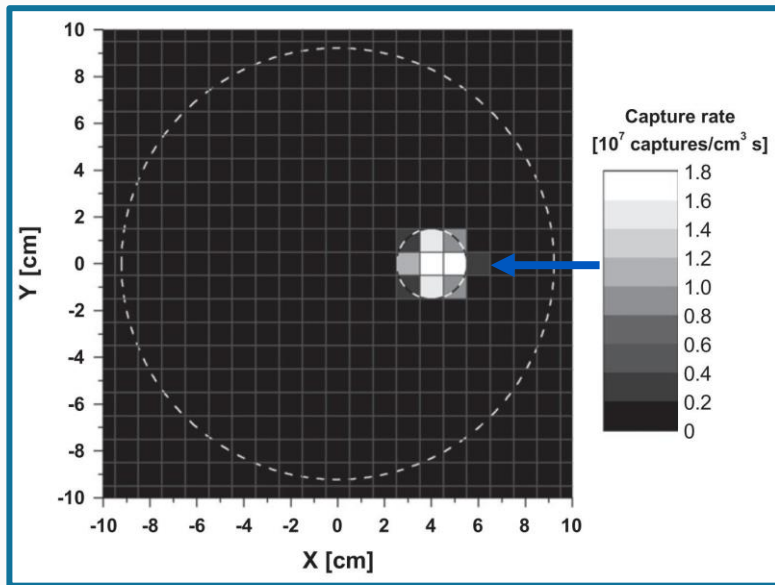


Fig 8. Tomographic image of boron neutron capture rate from Minsky et al [2].

- Tumour contained 400 ppm ^{10}B

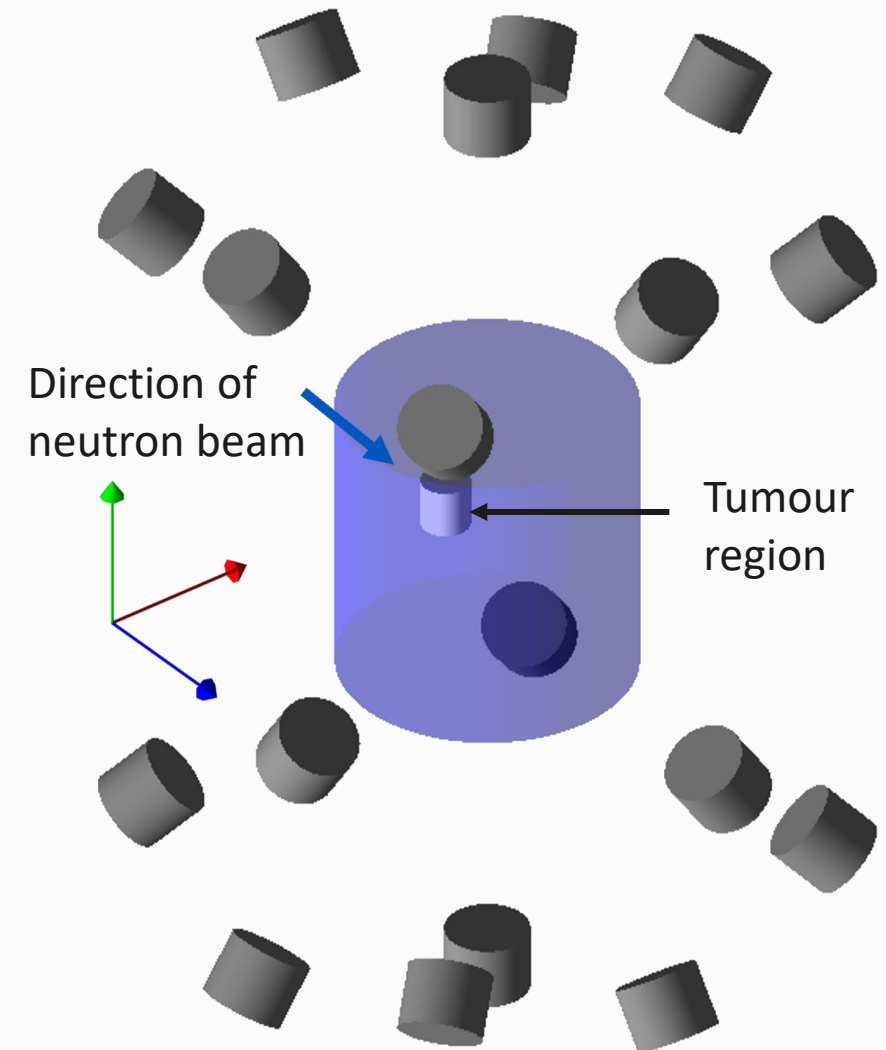
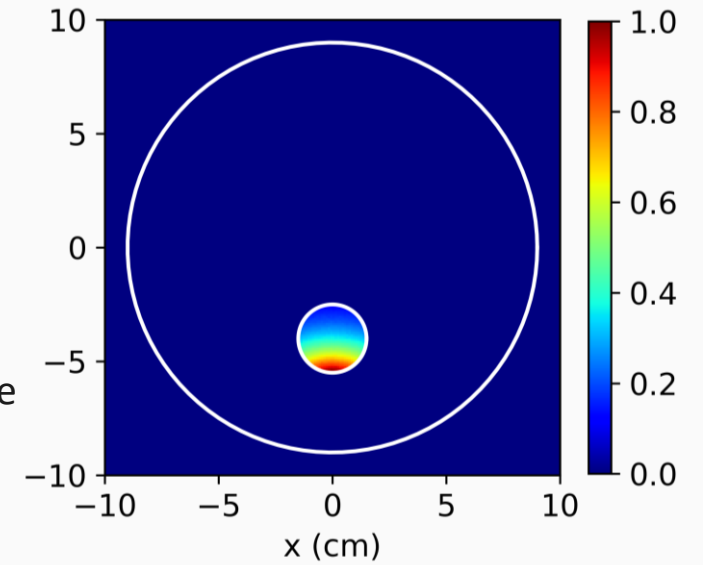


Fig 9. Visualisation of the phantom within the 18 detector array.

Reconstructed Images of Phantom

- True source of the 478 keV photons extracted from simulation

Fig 10. True distribution of the origin of the 478 keV photons.



Reconstructed Images of Phantom

- True source of the 478 keV photons extracted from simulation
- Reconstructed image clearly highlights the tumour region – highest intensity at bottom edge
- 0.004% absolute efficiency
- Further study would be required to quantify spatial resolution

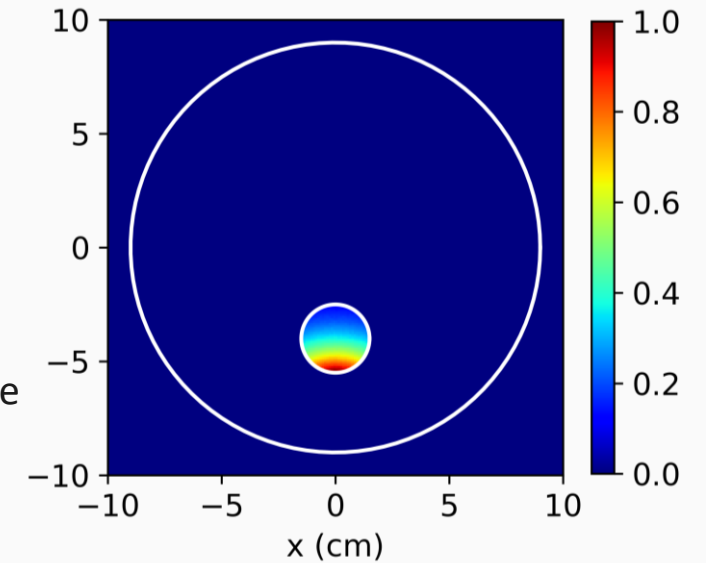


Fig 10. True distribution of the origin of the 478 keV photons.

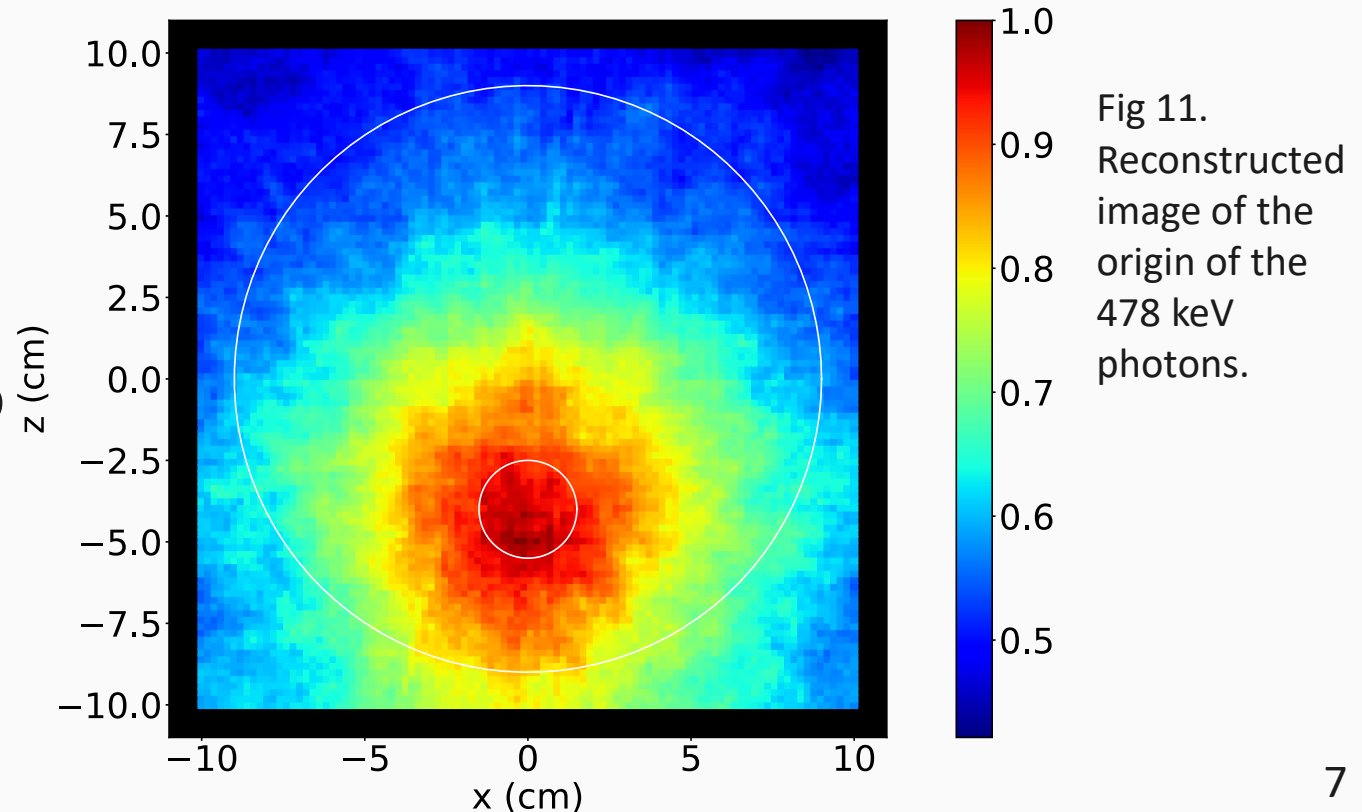


Fig 11. Reconstructed image of the origin of the 478 keV photons.

Simulation \longrightarrow Experimental Work

- Simulation study published in February 2024

K. Nutter, T. Price, Tz. Kokalova, S. Green, B. Phoenix. **A feasibility study using an array of $\text{LaBr}_3(\text{Ce})$ scintillation detectors as a Compton camera for prompt gamma imaging during BNCT.** *Frontiers in Physics* 12, 2024.

- Publication also covered investigation into impact of shielding
- Experimental work to validate the overall camera performance in the simulation was **desirable**

Experimental Setup

- Array of 10 LaBr_3 detectors available

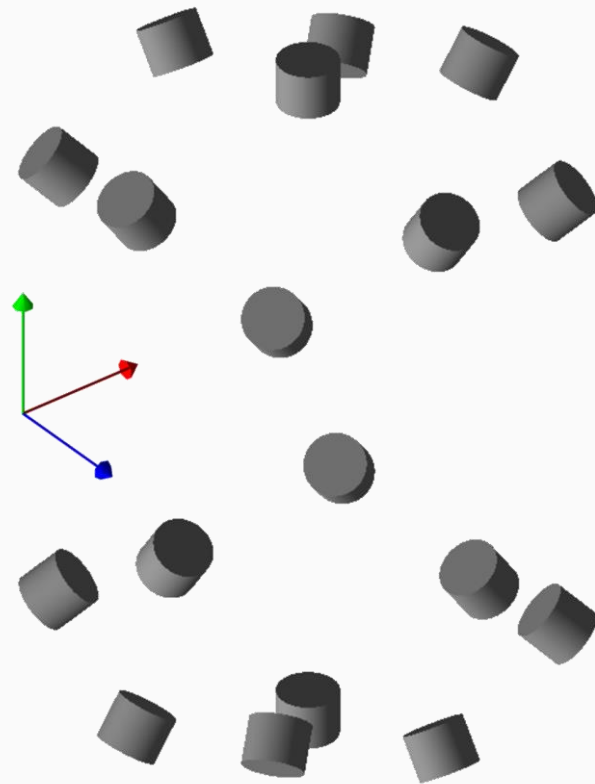


Fig 5. Extrapolated 18 detector array 30 cm from centre.

Experimental Setup

- Array of 10 LaBr_3 detectors available

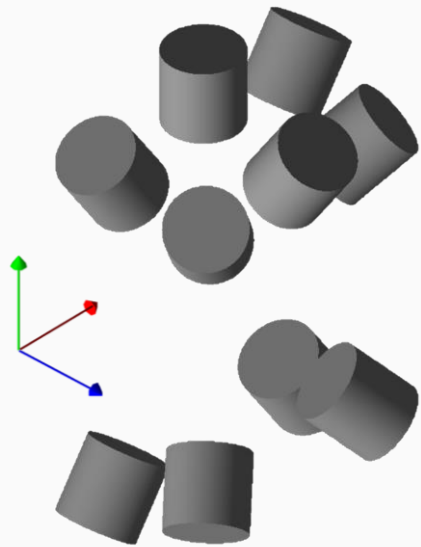


Fig 3. Original 10 detector array.

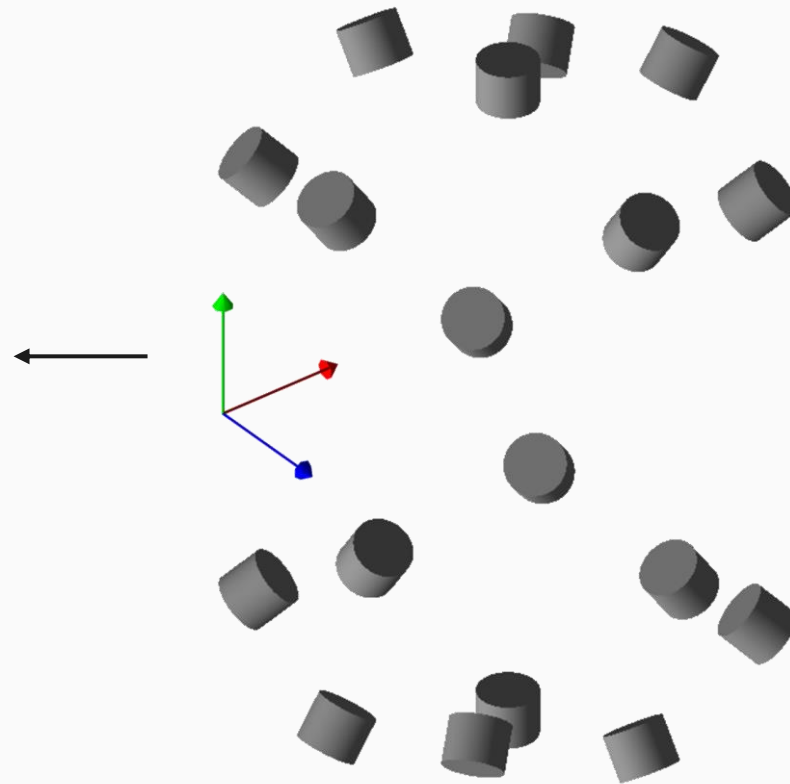


Fig 5. Extrapolated 18 detector array 30 cm from centre.

Experimental Setup

- Array of 10 LaBr₃ detectors available

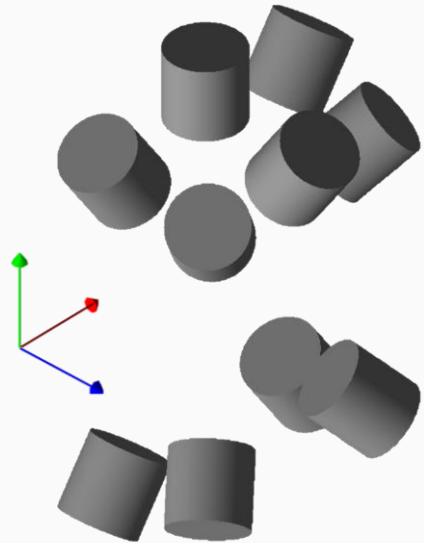


Fig 3. Original 10 detector array.

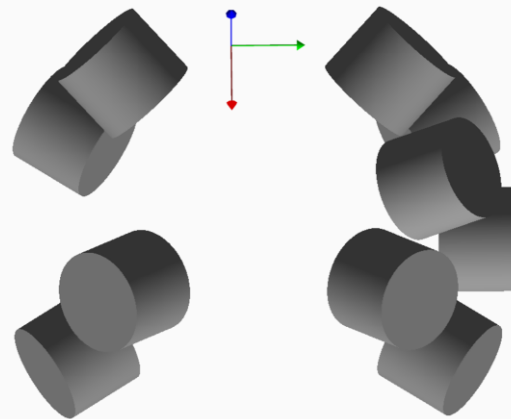


Fig 12. Rotated 10 detector array.

- All tests used ¹³⁷Cs as the source



Fig 13. Photograph of the experimental setup of the 10 detector array.

Experimental Results – 1 Central Source

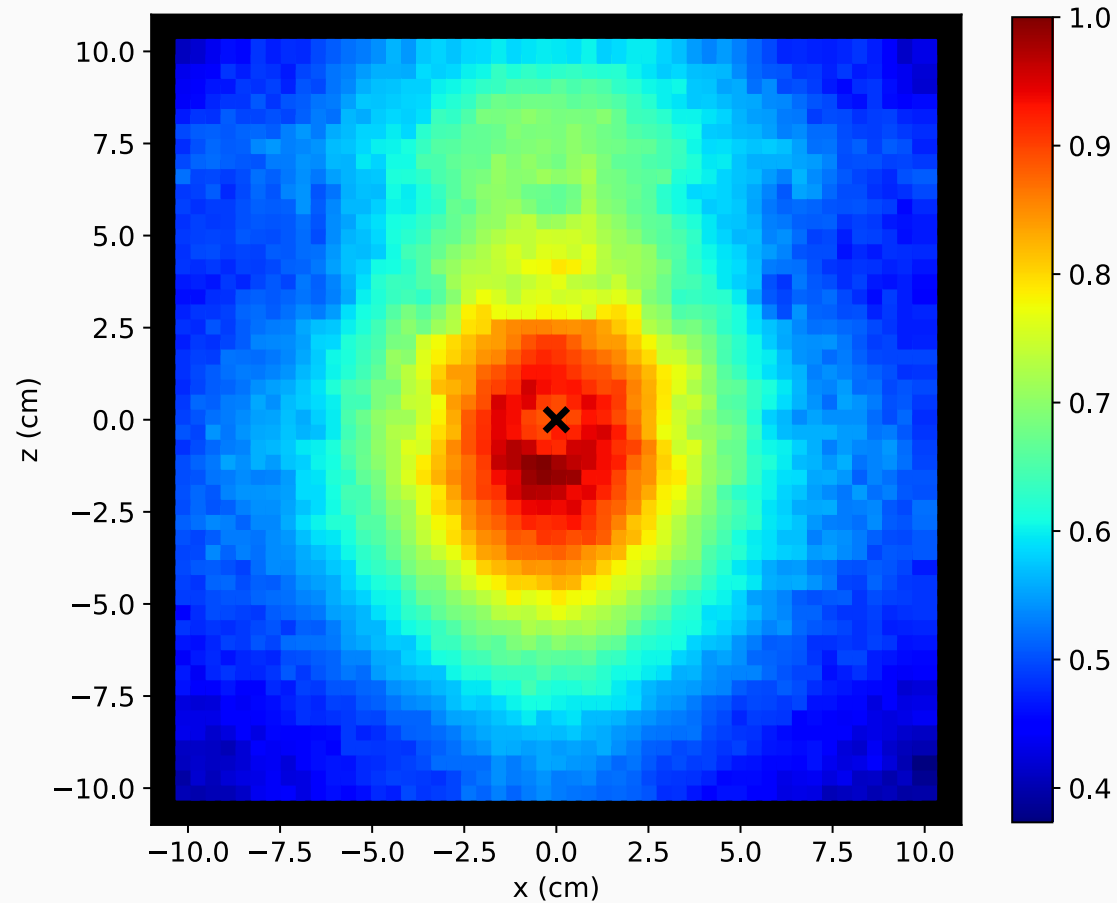


Fig 14. **Simulation image** of a central 662 keV point source.
Image displays the XZ plane at $y = 0$

Experimental Results – 1 Central Source

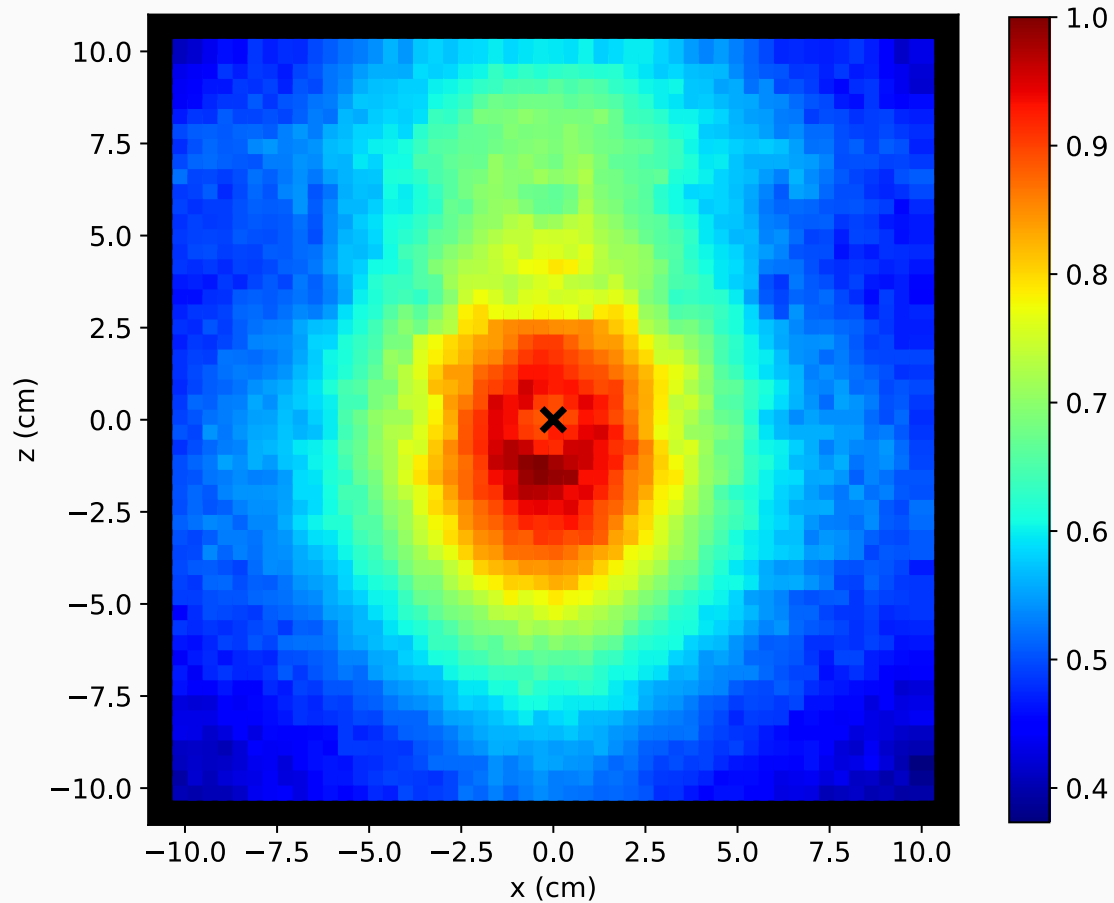


Fig 14. **Simulation image** of a central 662 keV point source. Image displays the XZ plane at $y = 0$

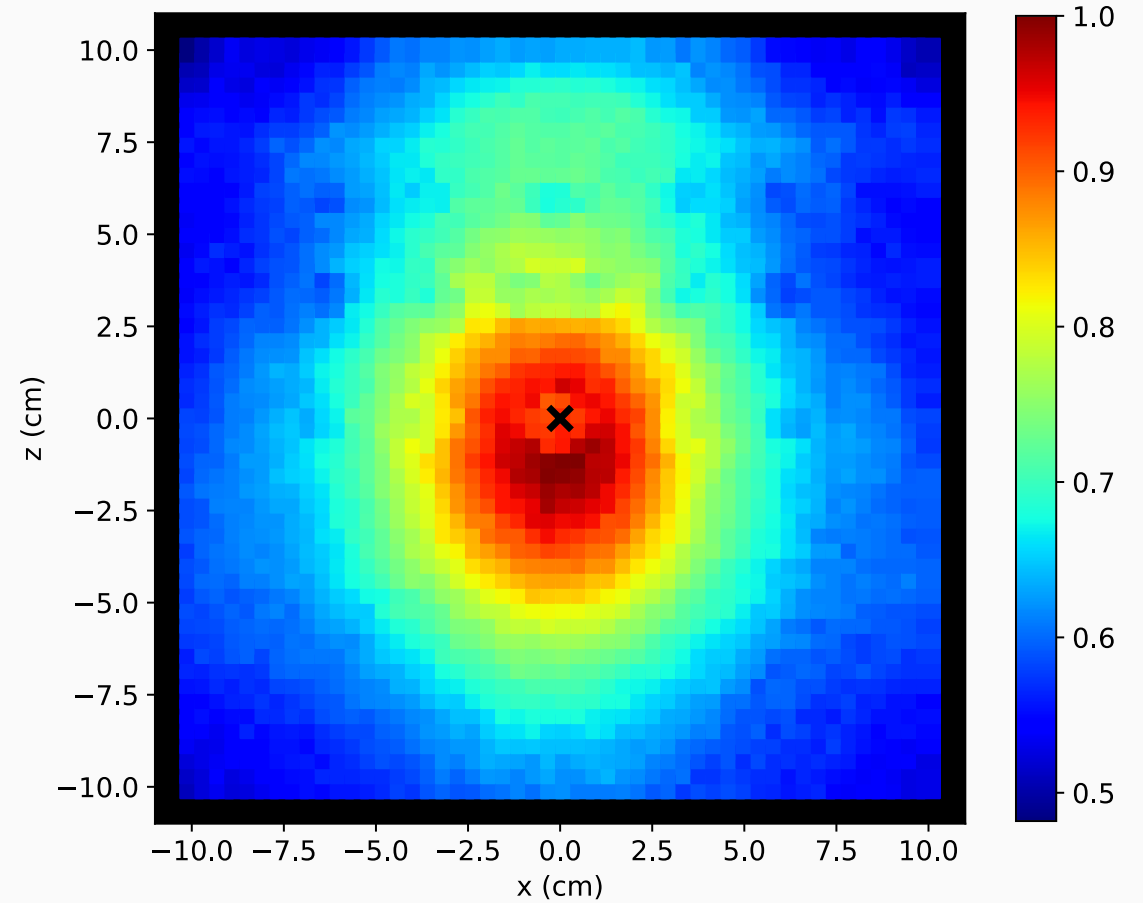


Fig 15. **Experimental image** of a central 662 keV point source. Image displays the XZ plane at $y = 0$

Spot the Difference!

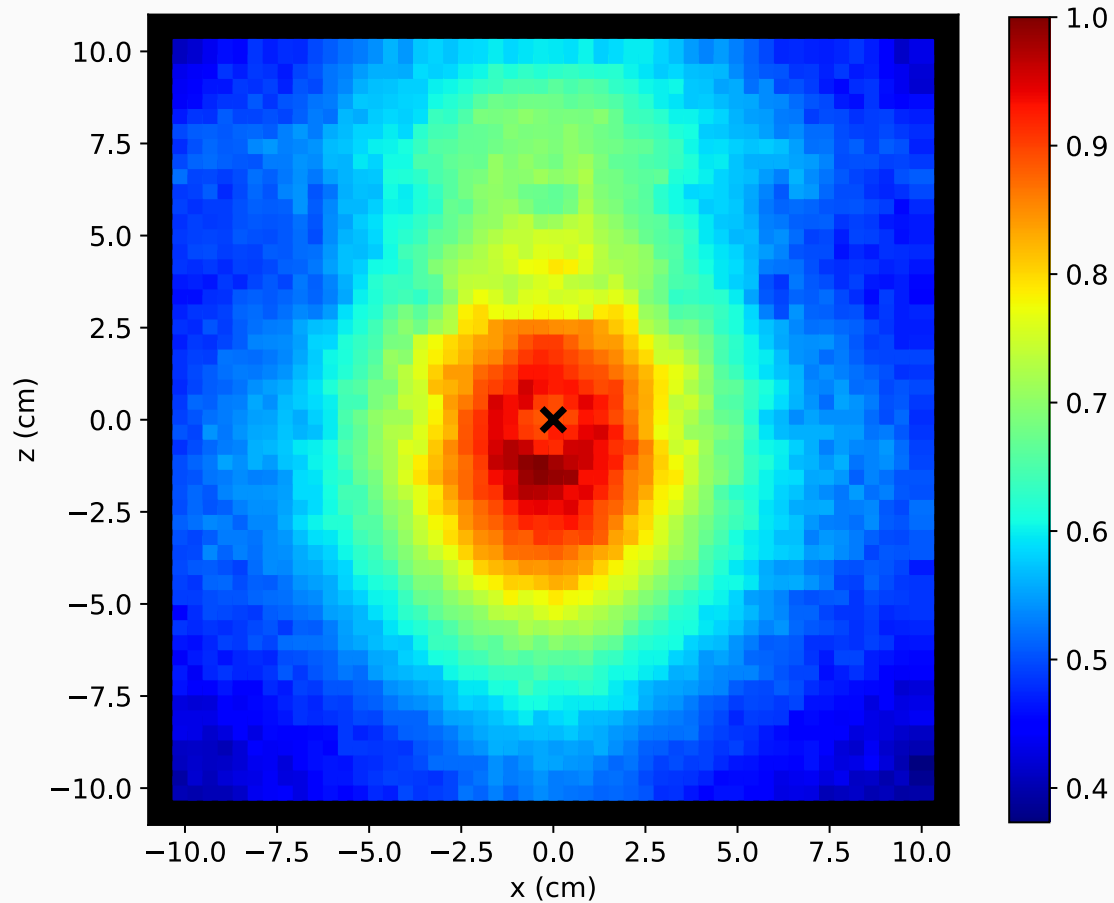


Fig 14. **Simulation image** of a central 662 keV point source. Image displays the XZ plane at $y = 0$

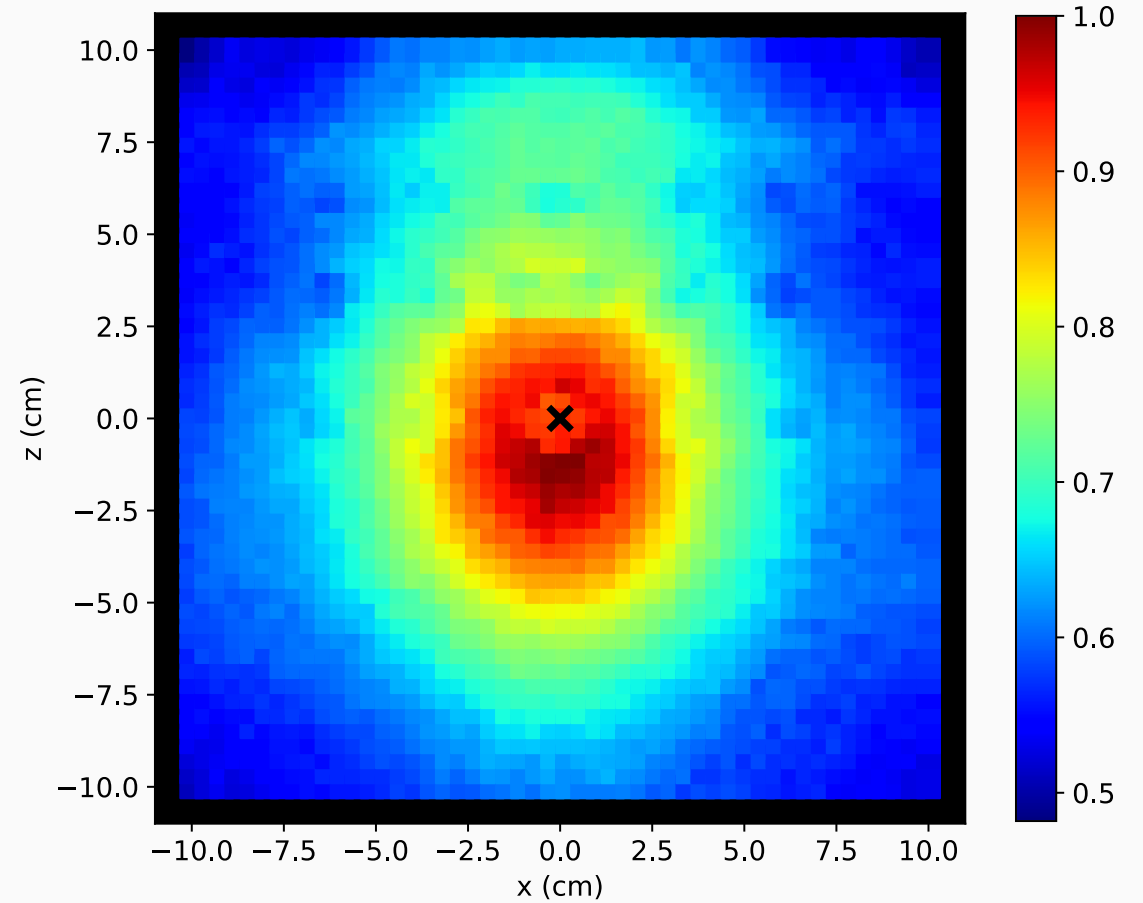


Fig 15. **Experimental image** of a central 662 keV point source. Image displays the XZ plane at $y = 0$

Spot the Difference!

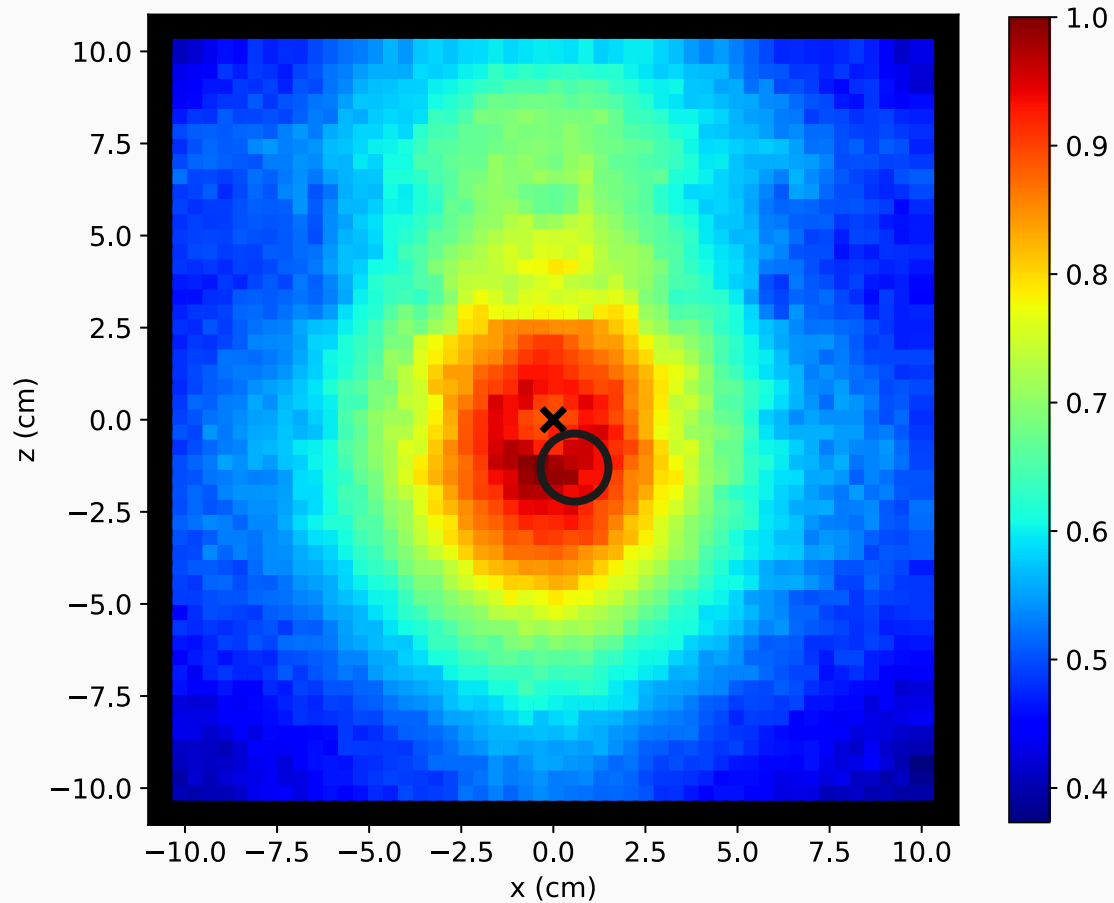


Fig 14. **Simulation image** of a central 662 keV point source. Image displays the XZ plane at $y = 0$

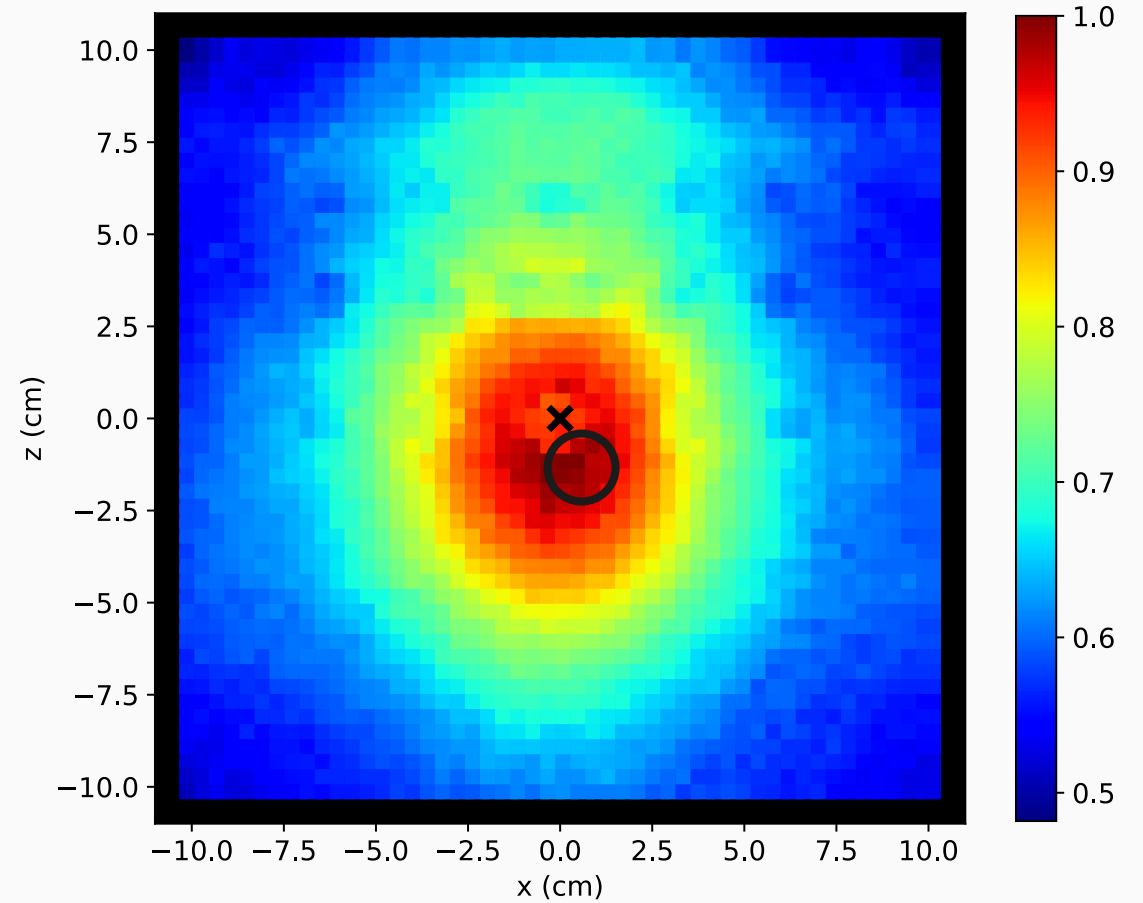


Fig 15. **Experimental image** of a central 662 keV point source. Image displays the XZ plane at $y = 0$

Spot the Difference!

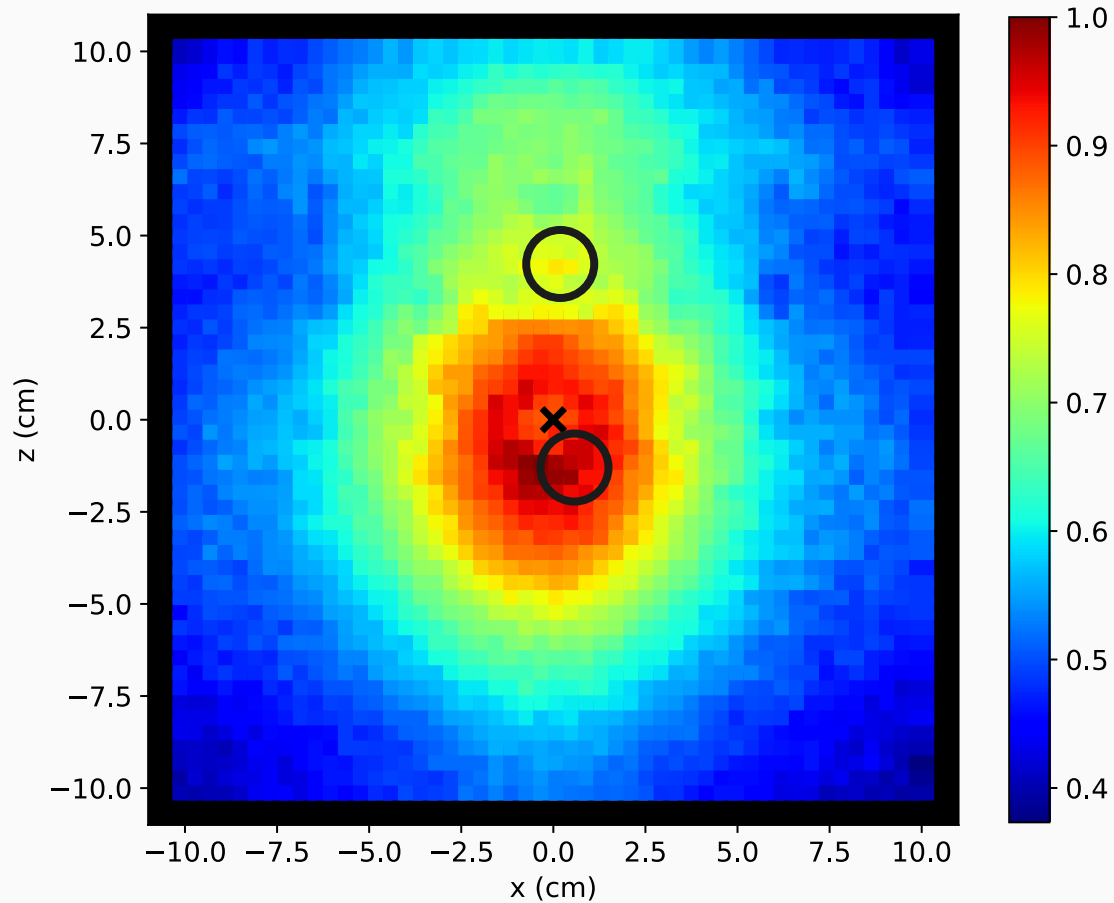


Fig 14. **Simulation image** of a central 662 keV point source. Image displays the XZ plane at $y = 0$

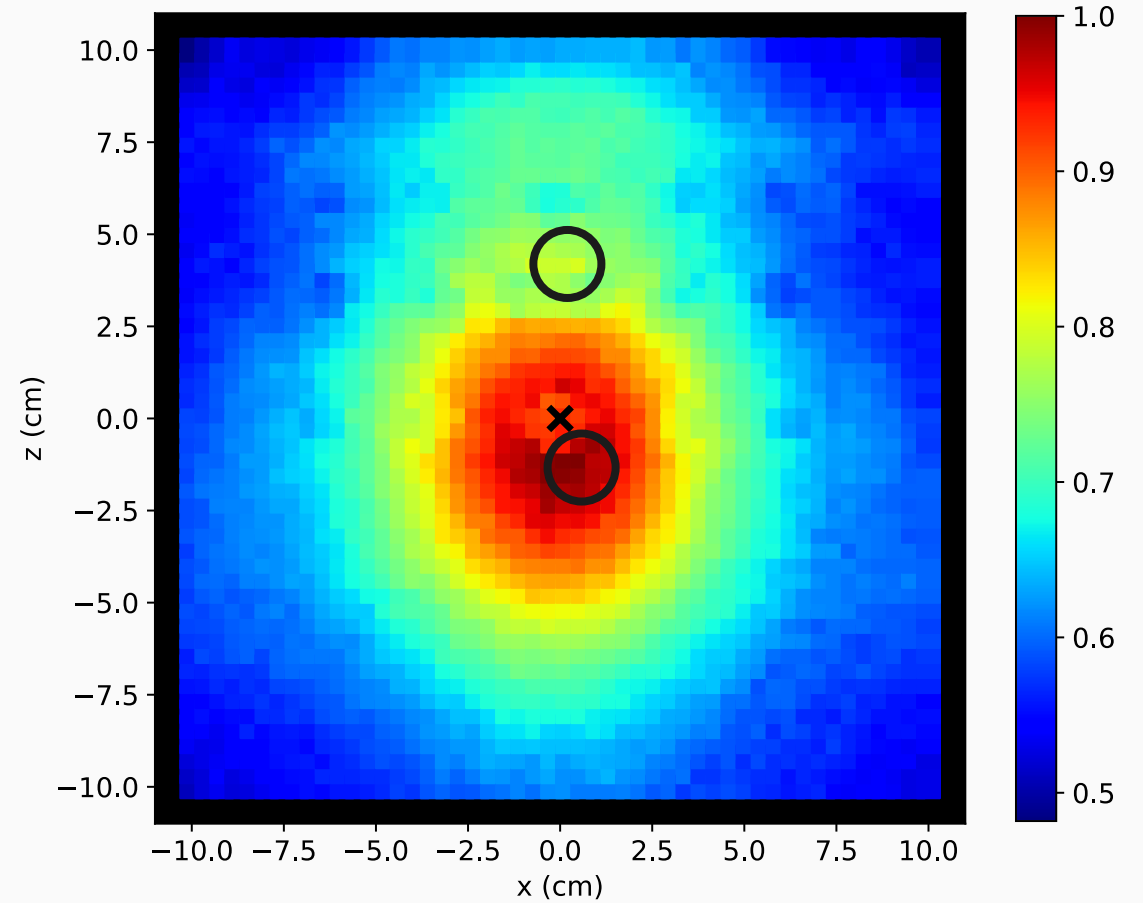


Fig 15. **Experimental image** of a central 662 keV point source. Image displays the XZ plane at $y = 0$

Spot the Difference!

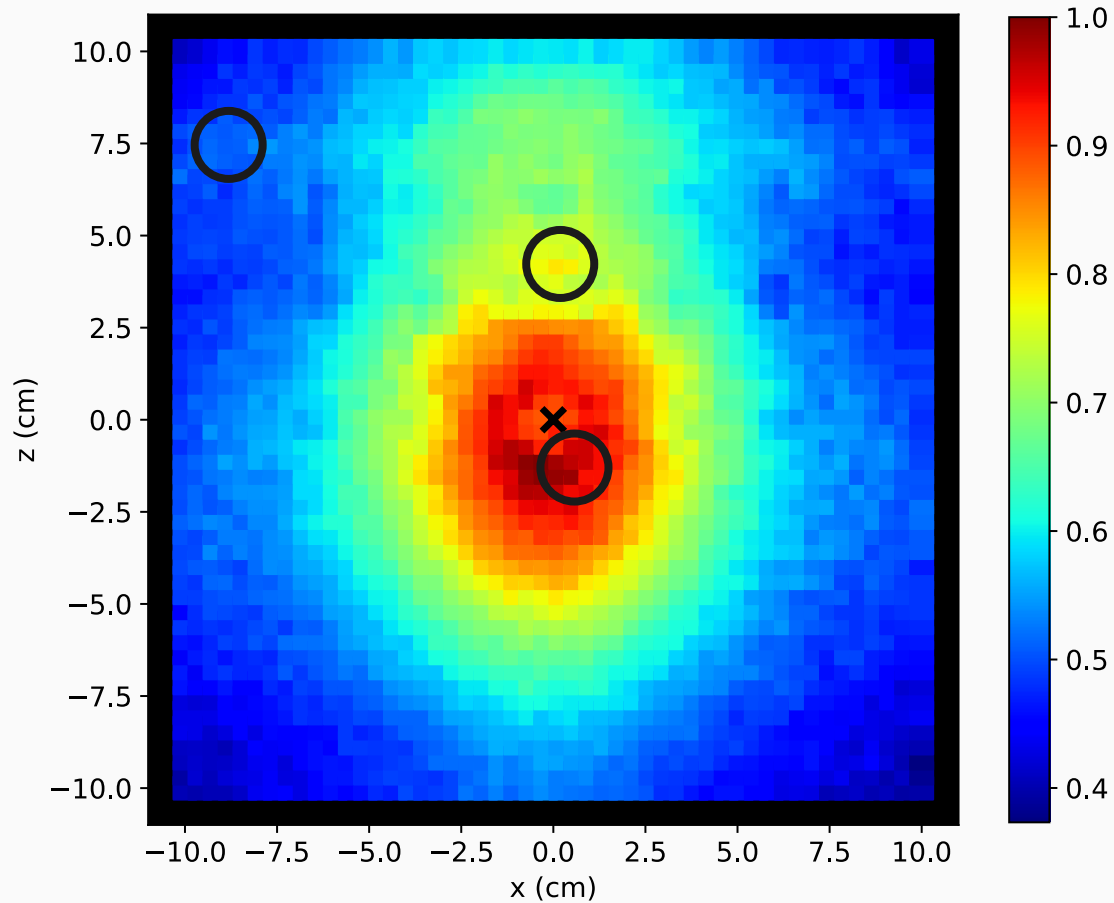


Fig 14. **Simulation image** of a central 662 keV point source. Image displays the XZ plane at $y = 0$

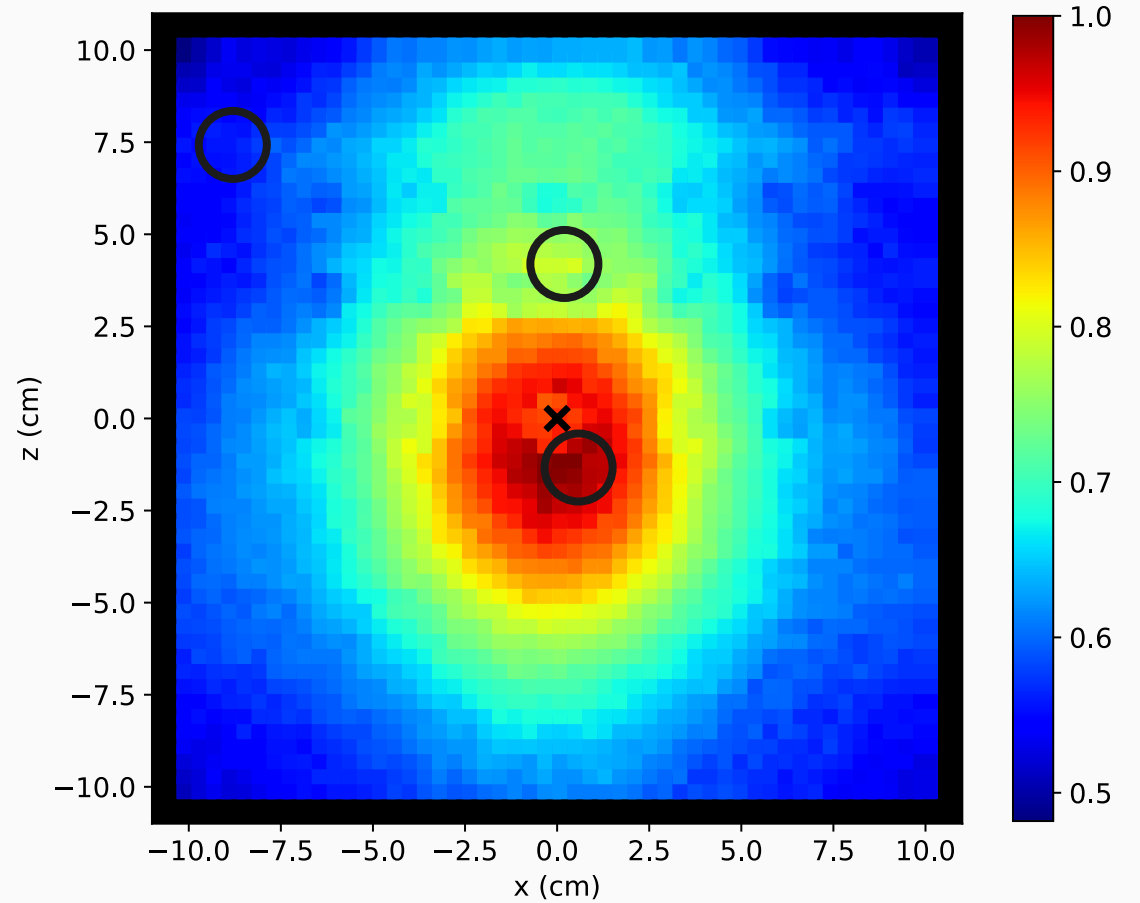


Fig 15. **Experimental image** of a central 662 keV point source. Image displays the XZ plane at $y = 0$

Experiment vs. Simulation – 1 Central Source

- The percentage difference for every pixel in the image can be found
- Provides **quantitative measure** of similarity between simulation and experimental images

Experiment vs. Simulation – 1 Central Source

- The percentage difference for every pixel in the image can be found
- Provides **quantitative measure** of similarity between simulation and experimental images
- Around the source location difference is $< 5\%$

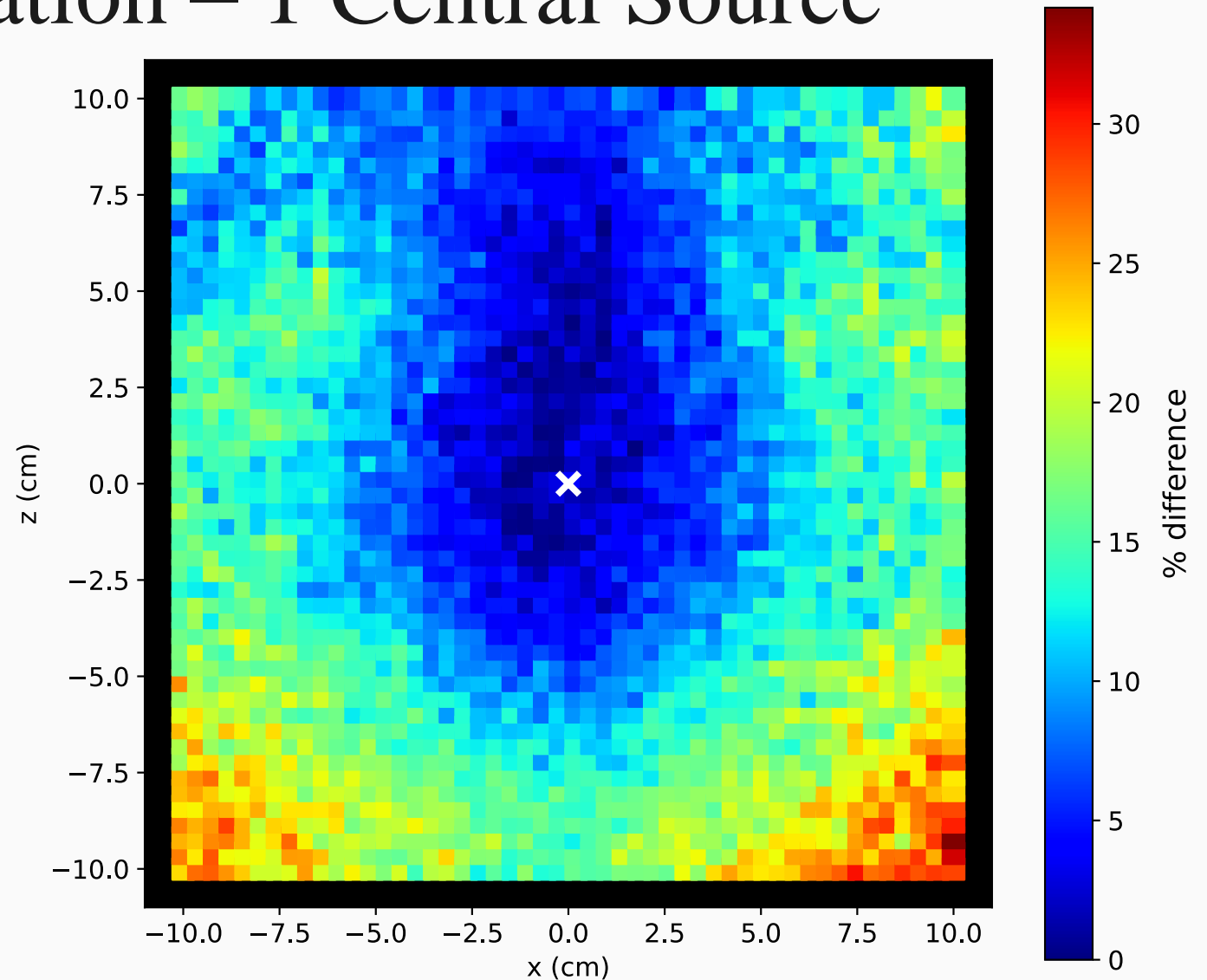


Fig 16. The **percentage difference** between the simulated and experimental images of **the central source** for each pixel in the plane.

Experimental Results – Two Sources

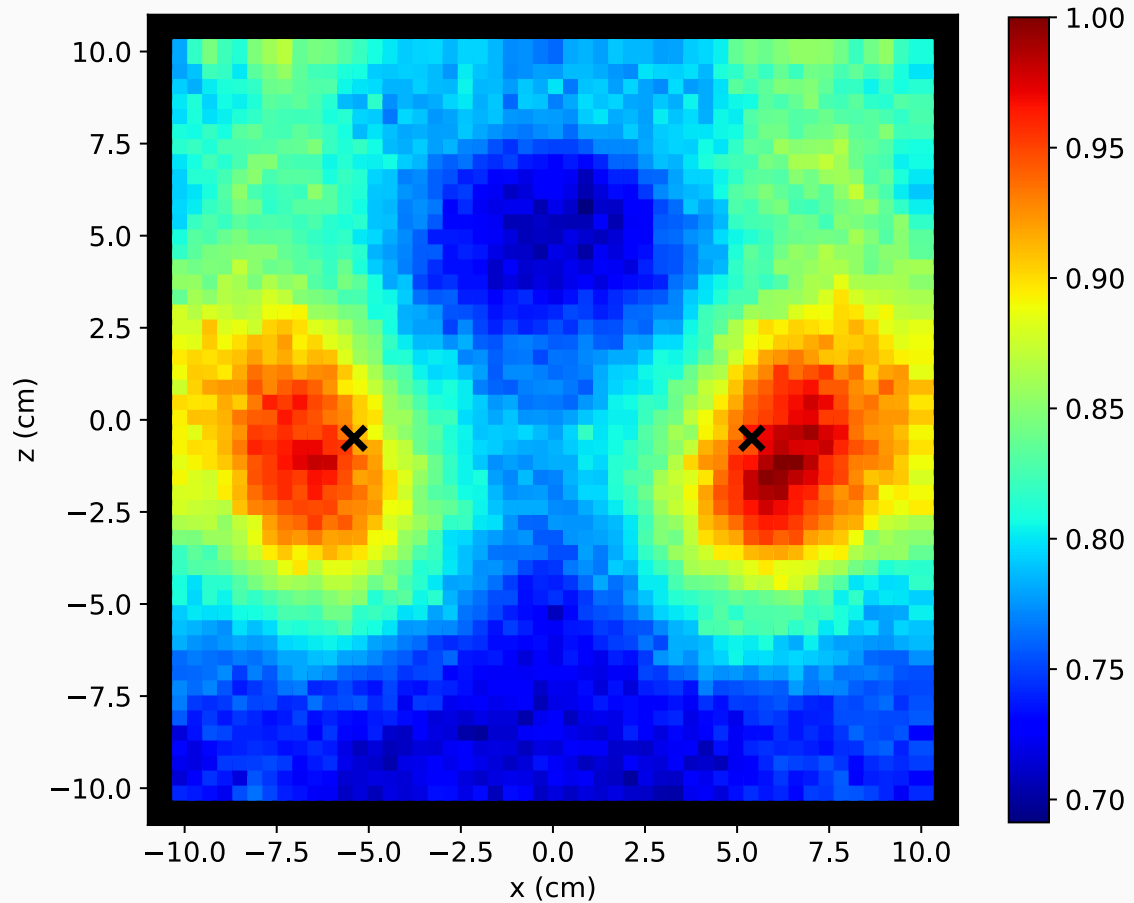


Fig 17. **Simulation image** of dual 662 keV point sources.
Image displays the XZ plane at $y = 0$

Experimental Results – Two Sources

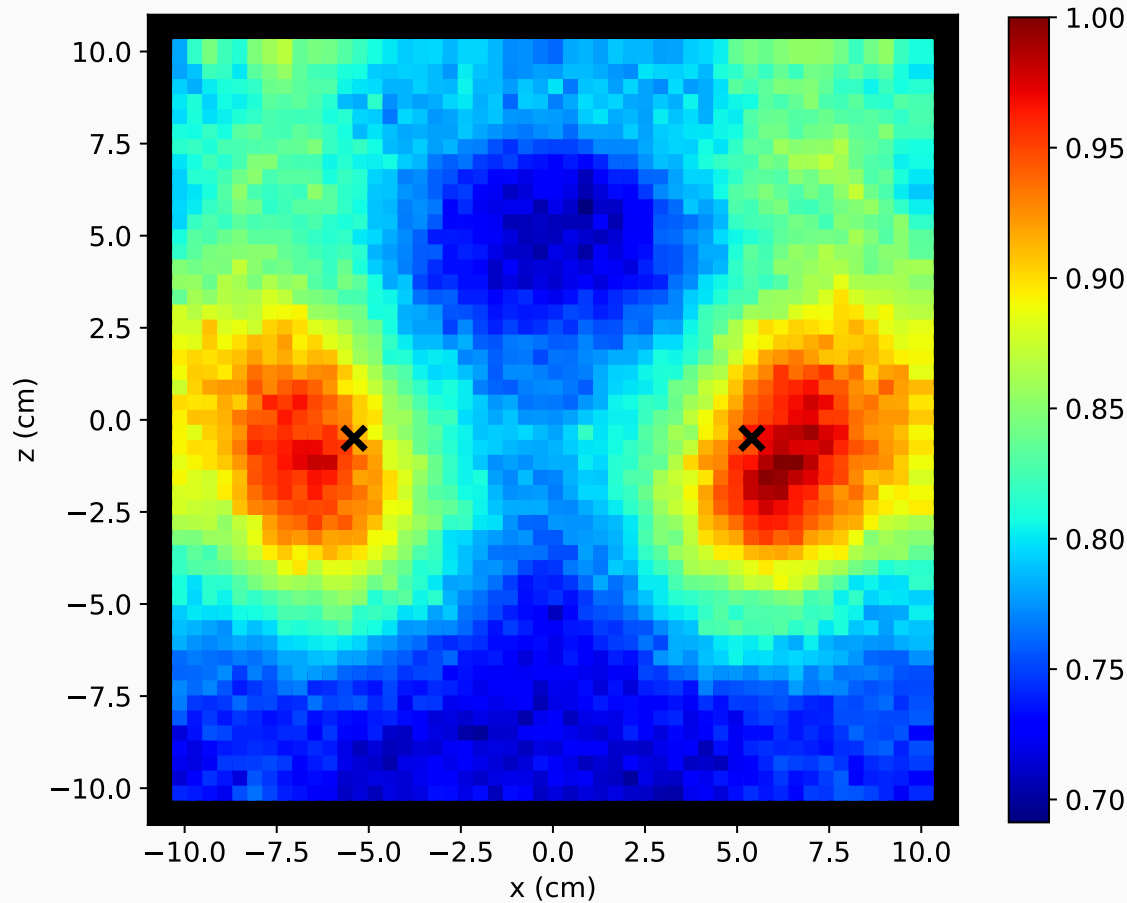


Fig 17. **Simulation image** of dual 662 keV point sources. Image displays the XZ plane at $y = 0$

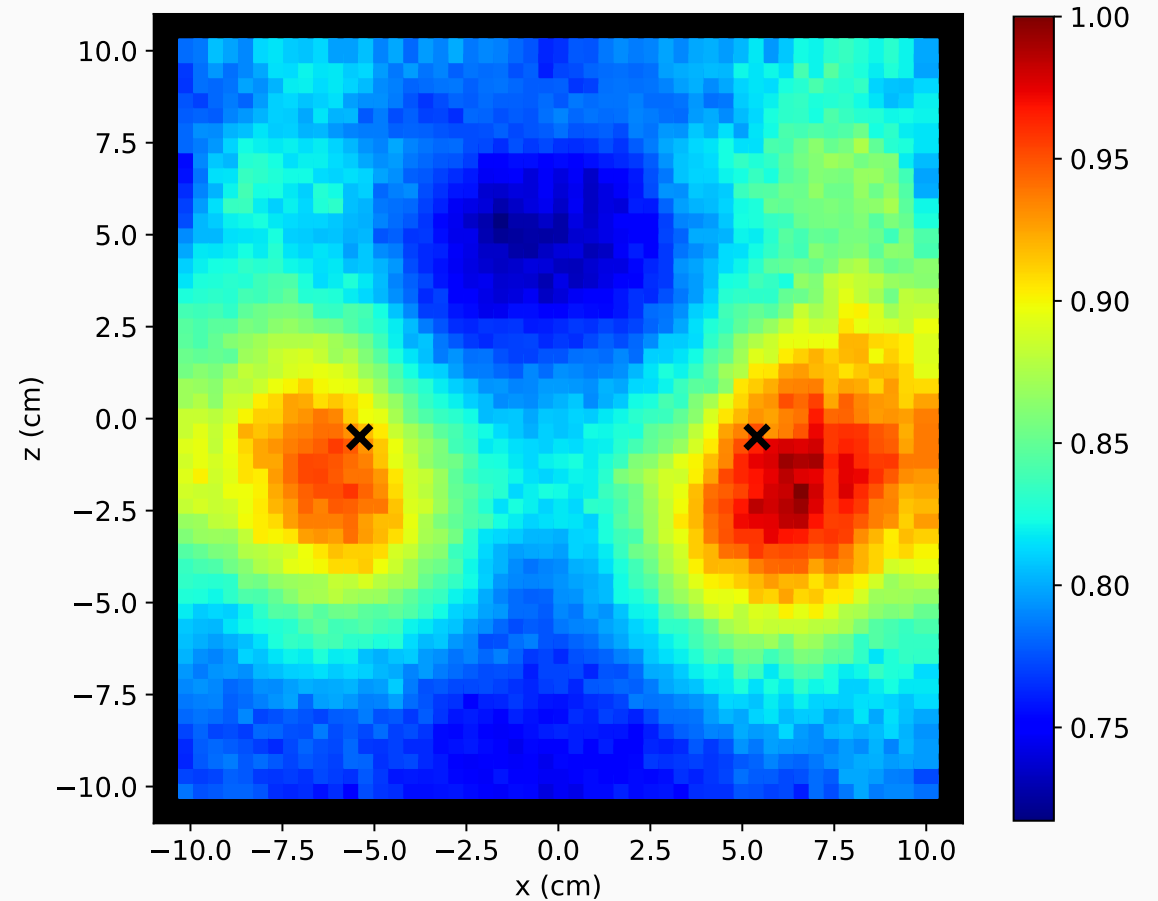


Fig 18. **Experimental image** of dual 662 keV point sources. Image displays the XZ plane at $y = 0$

Experiment vs. Simulation – Two Sources

- Again generally $< 5\%$ difference around the source locations

★ **Clear validation that the simulation behaves very similarly to the physical setup!**

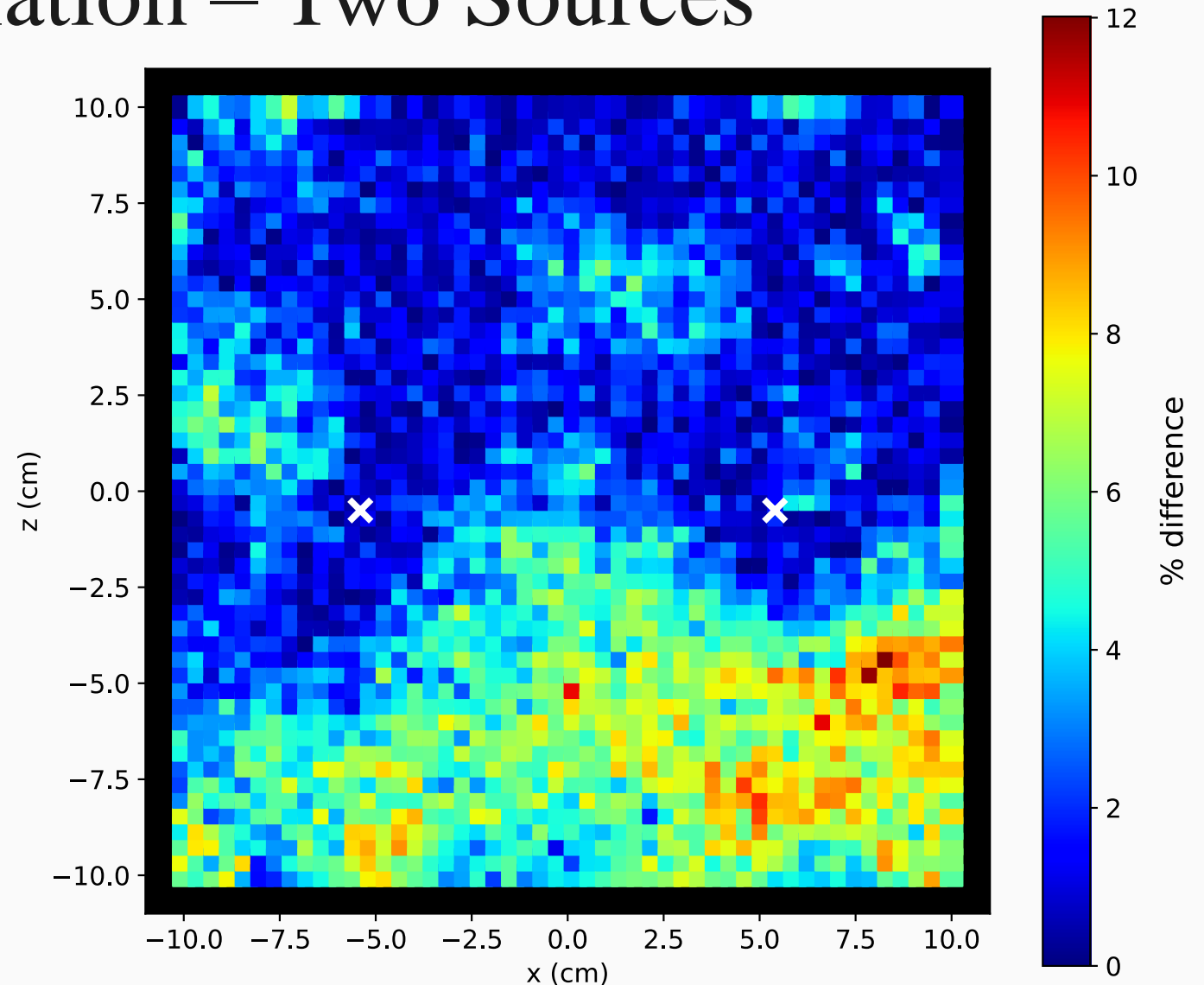


Fig 19. The **percentage difference** between the simulated and experimental images of **the dual sources** for each pixel in the plane.

Summary

- BNCT provides alternative cancer therapy with both biological and physical targeting of the tumour
- Dosimetry is challenging, but prompt gamma imaging could offer an online method
- **Simulation study using Geant4 showed feasibility of using a modified Compton camera design for prompt gamma imaging during BNCT**
- **Experimental work to validate the simulated camera performance demonstrated a very good agreement between simulation and experiment**